Cooperating Dinitrogen and Phenyl Rotations in *trans*-Azobenzene Photoisomerization

José A. Gámez,[†] Oliver Weingart,[‡] Axel Koslowski,[†] and Walter Thiel*[,†]

[†]Max-Planck-Institut für Kohlenforschung, Kaiser-Wilhelm-Platz 1, 45470 Mülheim an der Ruhr, Germany

[‡]Institut für Theoretische Chemie und Computerchemie, Heinrich-Heine-Universität Düsseldorf, Universitätsstrasse 1, 40225 Düsseldorf, Germany

S *Supporting Information*

ABSTRACT: Semiempirical OM2/MRCI surface-hopping simulations have been performed to study the *trans*-to-*cis* photoisomerization of azobenzene upon excitation to the S_1 state. The decay dynamics to the ground state shows an oscillatory pattern that can be attributed to an out-of-plane rotation of the N_2 moiety. The reaction is thus initially driven by N_2 rotation which triggers phenyl rotations around the C−N bonds. The *cis* isomer is produced most effectively when the phenyl rings rotate in phase. Mode-specific excitations cause variations in the computed decay times and product yields.

INTRODUCTION

The photoinduced *cis*−*trans* isomerization of azobenzene has been exploited extensively both for the construction of nanodevices and the synthesis of new nanomaterials. The molecular motion generated by this reaction can be transferred to the macroscopic scale. It has been used for the photo-orientation of liquid crystals[1−4] and the synthesis of polymers which can undergo photocontraction[5] and so produce mechanical work.[6,7] It has thus been utilized for making prototype molecular machines.[8,9] Moreover, azobenzene-based polymers have been designed whose viscosity can be controlled by light,[10−12] based on the (dis)ordering created by the isomerization process.

In spite of these numerous and novel applications, the detailed mechanism of azobenzene photoisomerization is still a subject of controversy. It has been extensively studied with experimental and theoretical methods. The reaction is ultrafast and involves two low-lying singlet excited states, namely S_1 and S_2. Interestingly, the two states show different quantum yields, and the reaction violates Kasha's rule.[13] Through steady-state measurements it has been shown that the yield of the *trans*-to-*cis* isomerization in hexane is 0.20−0.27 when exciting to the S_1 state but drops dramatically to 0.09−0.12 for the S_2 excitation.[14−16] Similarly, the quantum yield for the S_1 *cis*-to-*trans* reaction is higher (0.55−0.68), compared to the reaction in S_2 (0.40−0.44).[17−19] In this work we will focus on the S_1 state, as it shows the most efficient *cis*−*trans* interconversion.

The S_1 state is associated with a symmetry-forbidden $n−\pi^*$ transition in the visible region.[20−22] Traditionally, two mechanisms have been proposed for the photoisomerization of azobenzene: (i) rotation of the phenyl rings around the N−N moiety or (ii) inversion of the phenyl groups by varying the CNN angle without activation of the CNNC dihedral motion. Rau and co-workers measured the quantum yields of azobenzene and of derivatives, in which the rotation around the N═N double bond was blocked by a cyclophane structure[23] or a crown ether.[15] The results were practically the same for all three systems, and it was thus concluded that

the S_1 photoisomerization goes through an inversion mechanism. This was also supported by the experiments of Fujino et al.[24] and by early theoretical calculations.[25−27] More recent theoretical dynamical simulations[28−36] challenge this view and propose the rotation of the phenyl rings around the N═N bond as the main reaction coordinate. Pancur and co-workers came to a similar conclusion in their recent time-resolved fluorescence experiments.[37] They however pointed out that their measurements are also compatible with a mechanism where the phenyl rings are fixed and the N_2 moiety rotates. This motion is often referred as hula twist of the N atoms, in analogy to a similar mechanism proposed for the isomerization of stilbene.[38,39] Doltsinis et al.[40−42] observed a similar behavior. In their dynamical simulations, the phenyl rings remained nearly fixed in space, while the change in the CNNC dihedral was primarily produced by the rotation of the N═N bond. This latter mechanism is also supported by our recent work on the *cis*-to-*trans* photoisomerization of azobenzene.[43] By analyzing the periodic features of the decay to the ground state, we identified the N_2 rotation as the coordinate driving the reaction.

Apparently there is still a lack of consensus on how this reaction proceeds. By means of semiempirical nonadiabatic dynamical simulations, we aim for a better and more detailed mechanistic understanding that may be helpful for gaining control and modifying the course of this photoreaction. We focus on the processes initiated by excitation to the S_1 state, which gives the highest quantum yield. We also examine whether the *trans*-to-*cis* isomerization exhibits features similar to those found in our recent excited-state dynamics simulations of the *cis*-to-*trans* reaction.[43]

COMPUTATIONAL DETAILS

The potential energy surfaces (PES) involved in the photoreaction were generated using the OM2/MRCI semiempirical

Table 1. Excitation Energies and Geometries of the Stationary Points Relevant for tAB → cAB Photoisomerization[a]

	symmetry		OM2/MRCI	CASSCF	expt.	literature[f]
tAB (S$_0$)	C_{2h}	$\Delta E(n\pi^*)$	2.44	3.12	2.79[b], 2.82[c]	2.53–3.24
		d(N–N)	1.214	1.211	1.260[d]	1.230–1.279
		d(C–N)	1.448	1.429	1.427[d]	1.400–1.437
		∠CNN	116.2	115.7	113.6[d]	113.4–119.8
tAB (S$_1$)	C_{2h}	$\Delta E(n\pi^*)$	1.43	1.67		1.48–1.83
		d(N–N)	1.218	1.218		1.250–1.272
		d(C–N)	1.399	1.343		1.373–1.378
		∠CNN	130.6	131.7		126–129
cAB	C_2	$\Delta E(n\pi^*)$	3.13	3.33	2.92[b]	2.72–3.95
		d(N–N)	1.189	1.269	1.253[e]	1.210–1.274
		d(C–N)	1.448	1.441	1.449[e]	1.434–1.447
		∠CNN	123.1	122.2	121.9[e]	120.4–129.2
		θ(CNNC)	2.0	5.6	8.0[e]	0–12.0
		θ(CCNN)	55.5	60.5	53.3[e]	43.2–79.9
MECI	C_1	$\Delta E(n\pi^*)$	0.00	0.00		
		d(N–N)	1.213	1.280		1.263
		d(C–N)	1.410/1.431	1.468/1.380		1.358–1.370/1.400
		∠CNN	122.7/130.4	117.2/135.3		117–118/136
		θ(CNNC)	97.5	93.0		93–94
		θ(CCNN)	10.1/10.0	0.9/2.3		

[a]Excitation energies ΔE are given in eV, bond lengths in Å, and angles in degrees.. [b]Ref 69. [c]Ref 70. [d]Ref 71. [e]Ref 72. [f]Theoretical estimates taken from refs 34 and 73–76.

method, which has recently been shown to give realistic results for a variety of different photoinduced processes.[43–48] For this work, the same setup was employed as in our previous study on the *cis*-to-*trans* reaction.[43] A set of initial molecular orbitals (MO) was obtained by a restricted open-shell Hartree–Fock method (ROHF)[49] using the semiempirical OM2 Hamiltonian[50–52] with standard parameters, as implemented in the MNDO code.[53] The ROHF approach turned out to be more robust than a restricted HF treatment for the computation of excited-state properties of azobenzene. With this set of orbitals, multireference configuration interaction (MRCI) calculations[54] were performed with an active space comprising 10 orbitals. In the ROHF solution for the planar *trans*-isomer, these are the four highest doubly occupied π orbitals, the singly occupied nitrogen lone-pair orbital (HOMO in the closed-shell case), one singly occupied π orbital (LUMO in the closed-shell case), and the four lowest unoccupied π* orbitals. Three reference configurations were selected, i.e., the ROHF configuration with two singly occupied MOs and the two corresponding closed-shell determinants with doubly occupied HOMO and LUMO, respectively. The MRCI calculations included all configurations generated by single or double excitations from the reference configurations. All relevant minima were fully optimized using standard techniques and characterized by force constant calculations. Conical intersections[55] were located using a Lagrange–Newton algorithm for optimization.[56]

The excited-state dynamics were studied by surface-hopping simulations[57,58] with an empirical decoherence correction[59] (d = 0.1 hartree). The set of initial conditions (structures and velocities) was obtained by Wigner sampling.[60] Dynamics runs were initiated in the S$_1$ state. The nuclear motion was followed using the velocity Verlet algorithm[61] with a constant time step of 0.1 fs, and between two such steps, the time-dependent electronic Schrödinger equation was propagated in intervals of 0.001 fs. At each step, the OM2/MRCI energies and gradients of the two lowest singlet states were computed, and the corresponding full nonadiabatic coupling matrix element was

calculated analytically. In total, 1000 trajectories were run and followed for a maximum of 1200 fs. Photoproducts were determined by monitoring the CNNC torsion angle after the surface hop back to the ground state. To investigate the importance of particular vibrational modes in the reaction, we ran further simulations, each of them comprising ca. 300 trajectories, where one or two modes were vibrationally excited. In this case, the set of initial conditions was generated with a pseudo-Wigner distribution of the vibrational excited modes and a Wigner distribution of the modes in the vibrational ground level, as implemented in the NEWTON-X code.[62]

The general performance of the OM2/MRCI method for excited-state properties has been documented in a comprehensive validation study,[63] and we have discussed its accuracy for excited-state dynamics simulations in several recent studies, especially in the case of *cis*-azobenzene[43] and adenine.[47] To further assess the accuracy of our present semiempirical results for *trans*-azobenzene, complete active space self-consistent field (CASSCF) calculations were performed with the atomic natural orbital (ANO) basis set proposed by Pierloot et al.[64] contracted to C,N[3s2p1d]/H[2s1p], using the MOLCAS 7.4 package of programs.[65] The electronic density resulting from the CASSCF calculations was analyzed using the electron localization function (ELF) proposed by Becke and Edgecombe.[66] Such analyses are useful for understanding the nature of the S$_0$ and S$_1$ states and, consequently, the evolution of the system with time. ELF is a function which measures the probability of finding an electron pair at a given region of the molecular space. Large values of ELF identify regions where electron pairs are localized, either as bonding or lone pairs. With the appropriate Lorentzian transform, ELF can be confined to the [0,1] interval, which facilitates the partitioning of the molecular space in polysynaptic (generally disynaptic) basins, with the participation of two (or more) atomic valence shells, and monosynaptic ones, which correspond to core electrons or lone pairs.[67] ELF grids and basin integrations were evaluated with the DGrid package.[68]

B

dx.doi.org/10.1021/ct300303s | J. Chem. Theory Comput. XXXX, XXX, XXX–XXX

■ RESULTS AND DISCUSSION

We follow the photoisomerization of *trans*-azobenzene (*t*AB) in the S_1 state. After vertical photoexcitation, *t*AB relaxes from the Franck—Condon geometry toward the S_1 minimum and then proceeds toward an S_1/S_0 intersection that acts as a funnel to the ground state, leading either to the *cis*-azobenzene (*c*AB) or back to the starting material. Energetically, there is an initial steep decrease in the potential energy by ca. 10 kcal mol^{-1}, which corresponds to the energy difference between the Franck—Condon geometry and the S_1 minimum. Due to its kinetic energy, *t*AB is not trapped in the region of the S_1 minimum but evolves in an almost barrierless process toward the crossing seam (see Supporting Information). No transition state could be located on the S_1 surface, because all such optimization attempts consistently led to S_0/S_1 crossing point structures.

Table 1 lists the geometries of the four relevant stationary points, i.e., the S_0 *t*AB equilibrium geometry, the S_1 *t*AB minimum, the S_1/S_0 minimum energy conical intersection (MECI), and finally the *c*AB ground-state minimum. *t*AB is planar and has C_{2h} symmetry both in the ground and the first excited state, while *c*AB has only C_2 symmetry; the MECI is unsymmetrical. The OM2/MRCI values in Table 1 are in reasonable agreement with ab initio CASSCF results and experimental data, suggesting that the OM2/MRCI approach can properly describe the photoinduced processes in azobenzene.

Among the species in Table 1, the most important one from a photochemical point of view is the MECI. It has a CNNC dihedral close to 90°, intermediate between the values of 180° in *t*AB and ca. 0° in *c*AB. In contrast to the three minima, the MECI is unsymmetrical since the two C—N distances, CNN angles, and CCNN dihedrals differ. More importantly, this structure shows helical chirality due to the helicity along the CCNNCC motif (see Figure 1).[77] This type of chirality is also
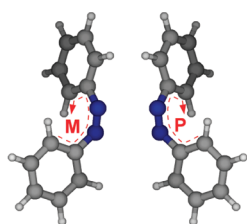

Figure 1. The two helical enantiomers of the MECI structure. The sign of the helical rotation along the CCNNCC motif determines the type of enantiomer.

present in *c*AB but not in planar *t*AB. For assignment, one has to look along the CCNNCC chain of the helix, with one phenyl ring in front and the other one in the back. Moving along the chain from the front to the back yields either a clockwise rotational motion (P or plus helicity, positive CNNC dihedral) or an anticlockwise rotational motion (M or minus helicity, negative CNNC dihedral). As a result there exist four different but degenerate MECIs.[43] Having two helical MECI enantiomers is relevant for the reactivity because this creates two different chiral pathways. We have recently shown that the *cis*-to-*trans* photoisomerization of azobenzene is enantioselective because the P-*c*AB preferentially evolves toward the P-MECI.[43]

However, such enantioselectivity is not expected in the *trans*-to-*cis* isomerization. The reaction starts from the planar *trans* structure, and energetically it does not make any difference

whether the rotation toward *cis* proceeds in plus or minus direction. Nonadiabatic dynamical simulations confirm this expectation (Figure 2). Starting from *t*AB, the trajectories are
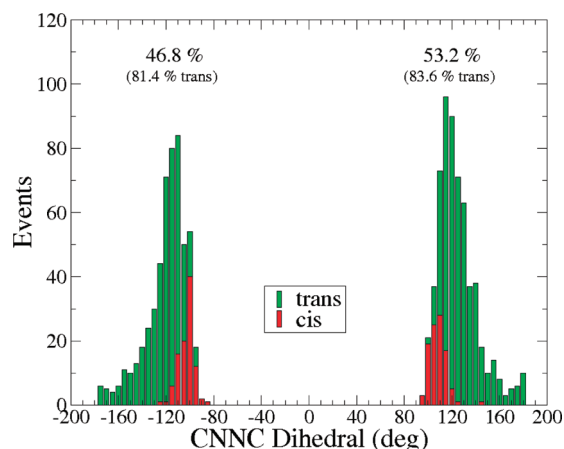

Figure 2. Distribution of the CNNC dihedral angles at the hopping structures. Negative (positive) dihedrals correspond to the M-helical (P-helical) pathway. Trajectories yielding *t*AB are shown in green, those yielding *c*AB in red.

distributed essentially equally between the M-helical and P-helical pathways (taking into account their limited number), indicating the lack of enantioselectivity. Figure 2 shows that *c*AB is produced by hopping events within a narrow window of CNNC dihedral angles (80°−120°) centered at the value of 97° for the MECI, while *t*AB is generated through hops at any CNNC dihedral angle larger than 80°. The *cis* isomer is thus obtained through hops close to the bottom of the (S_1/S_0) seam, i.e., close to the MECI, while the *trans* isomer is often accessed also by hops closer to the initial structure. This explains the low computed quantum yield of 17% *cis* isomer, which is in close agreement with the values of 20−25% determined experimentally.[14,15]

Dynamics simulations also provide information on the reaction rates. Figure 3 shows the distribution of hopping times. It is apparent that trajectories leading to *t*AB hop earlier to the ground state than those leading to *c*AB. This is reflected in the average hopping times of 247 fs for *trans* and 312 fs for *cis*, respectively. This difference is probably due to the fact that the *c*AB-trajectories hop to the ground state only through a rather small region of the (S_1/S_0) seam (see above). The
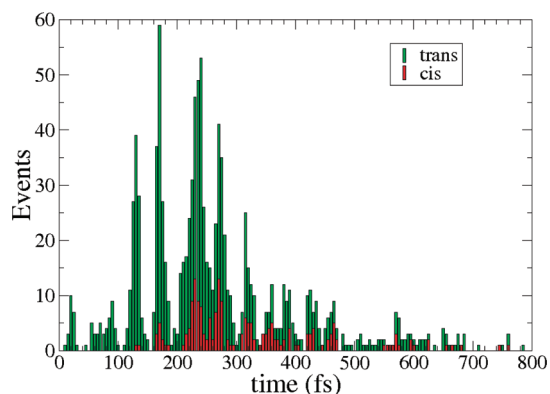

Figure 3. Distribution of hopping times for the *trans* → *cis* photoisomerization of azobenzene.

overall average decay time is 258 fs, which slightly underestimates the experimental value of 340 fs.[78] Interestingly, the hopping time distribution shows several maxima of hopping events spaced by 30−60 fs, suggesting some oscillatory feature in the decay to S_0.

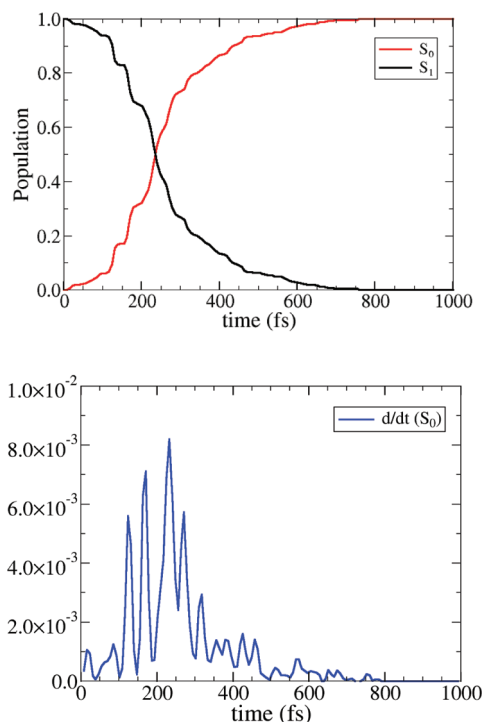The time evolution of the excited- and ground-state populations is shown in Figure 4. The decay to S_0 is not

Figure 4. Evolution of the S_0 and S_1 state populations (top) and derivative of the population of the S_0 state (bottom).

purely exponential: the curve has steep parts and small plateaus, which manifest themselves as peaks and valleys in the derivative of the S_0 population. Not surprisingly, the derivative graph shows the same oscillatory pattern as found in the hopping time distribution. A better understanding of these periodic features can be obtained by representing the derivative of the S_0 population in the frequency domain. A Fourier transform of

this function reveals a single signal of 338 cm^{-1}, i.e., there is a periodic movement of the molecule which appears to control the decay to the ground state. In fact, the S_1 minimum of *trans*-azobenzene has a vibrational mode of 342 cm^{-1} (OM2/MRCI) that corresponds to a rotation of the N_2 moiety out of the molecular plane, with concomitant variations of the CNNC and CCNN dihedrals. The N_2 rotation is also the major component of the vectors defining the branching space of the MECI (Figure 5). Analogous features were observed in our previous study of the *cis-to-trans* photoreaction: the decay to the ground state showed a similar oscillatory pattern, with a frequency close to that of the vibrational motion related to the out-of-plane N_2 rotation.[43] These findings stress the importance of decay function analysis as a useful tool for identifying important modes of reaction.

These observations suggest that the rotation of the N−N moiety modulates the approach to the crossing seam and the passage to the ground state. The twist of the N−N bond produces a variation in CNNC and CCNN dihedrals, while pulling on the phenyl rings. Thus, the overall "pedal motion"[40−42] during the initial stages of the *trans-to-cis* conversion is driven by the movement of the N−N moiety rather than the phenyl rings. This motion leads the trajectories toward the (S_1/S_0) crossing seam, and a (small) fraction of them will hop to the ground state during the first approach to the seam. The remaining trajectories will then oscillate in regions close to the seam and approach it again in subsequent vibrations, thus creating the observed oscillatory decay pattern (Figure 3).

We now consider in more detail the variation of the CNNC and CCNN dihedrals during the *trans-to-cis* conversion. These angles change overall from 180° to 2° and from 0° to 55°, respectively. To follow these changes during the reaction, we ran a trajectory at very low temperature and with no initial velocity to mimic the minimum energy path (MEP). We chose 20 K as a constant temperature for the trajectory, being the lowest value at which we could run technically satisfactory dynamics (no classical nuclear motion at 0 K, convergence problems at 10 K). The evolution of key dihedral angles along this trajectory is shown in Figure 6. Obviously the absolute CNNC dihedral value remains around 180° (*trans*) for some time and then gradually decreases toward 100° (typical of the seam region), while the CCNN dihedrals remain rather
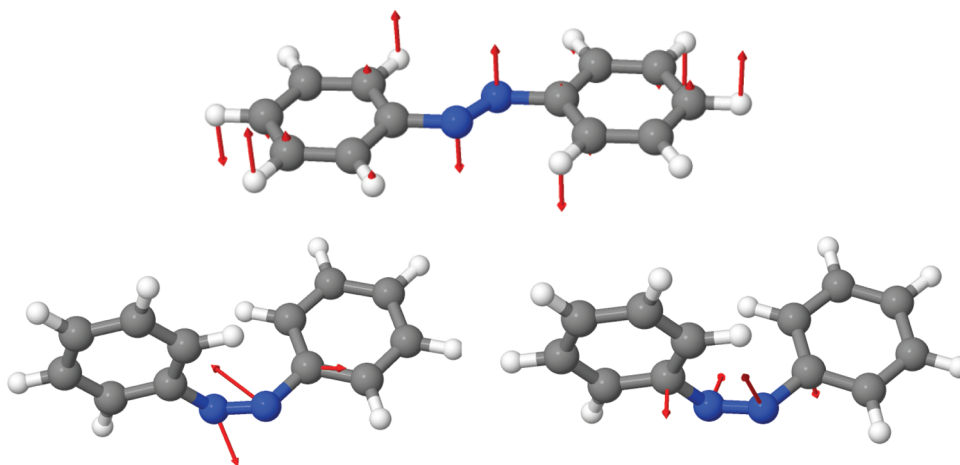

Figure 5. Vibrational mode (OM2/MRCI, 342 cm^{-1}) of the S_1 minimum of *t*AB (top) and derivative coupling (bottom-left) and energy gradient difference (bottom-right) vectors of the MECI.
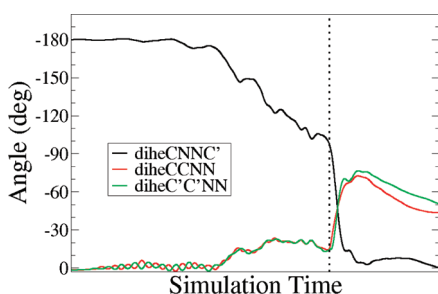
Figure 6. Evolution of CNNC and CCNN dihedrals along a trajectory run at a constant temperature of 20 K. The vertical dotted line indicates the hop to the ground state.

unperturbed and small. It is not until the system hops to the ground state that these CCNN dihedrals start to vary and to relax to the optimum value for the *cis* isomer. The same pattern has been found in other randomly selected trajectories yielding the *cis* photoproduct. This behavior is fully consistent with the small CCNN dihedral angles at the MECI structure (ca. 10°, see Table 1), which are close to those of the *t*AB.

What is the origin of such stage-wise structural variation? Both in the S_0 and S_1 state, *t*AB is a planar molecule of C_{2h} symmetry, but the S_1 minimum has slightly shorter C−N bonds and wider CNN angles compared with the S_0 structure (Table 1). The S_1 state corresponds to a HOMO → LUMO transition. The main contributions to the HOMO come from the nitrogen lone pairs and the N−N σ bond, while the LUMO is an antibonding π^* orbital located mainly at the N−N fragment, with small components at the phenyl rings (see Supporting Information). These MO compositions explain the slight increase of the computed N−N bond length but not the predicted significant shortening of the C−N bonds upon excitation (see Table 1). The topology of the ELF function can be used to further analyze the nature of these two states and the origin of the geometrical distortions upon excitation.

The complete ELF topology of azobenzene is presented in the Supporting Information. Figure 7 focuses only on the
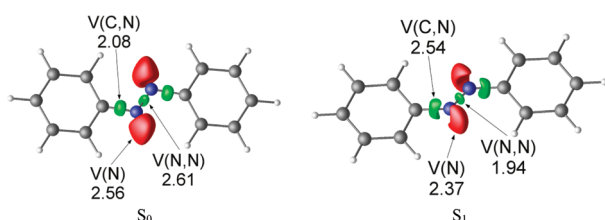

Figure 7. Localization domains of the ELF of azobenzene (ELF = 0.85) obtained with CASSCF densities of the S_0 (left) and S_1 (right) state. Green lobes refer to disynaptic basins between two bonding atoms, and red ones refer to monosynaptic lone-pair basins. The population of the different basins is given in units of electron charge. Color code: nitrogen in blue, carbon in gray, and hydrogen in white.

CNNC region and illustrates the situation upon excitation. There is a decrease of electron population in the V(N) and V(N,N) basins, while the V(C,N) basin populations increase, reflecting a charge transfer from the nitrogen lone pairs and N−N bonding region to the phenyl rings. In other words, the excitation produces a weakening of the N−N bond while reinforcing the C−N bonds. Contrary to the MO picture, ELF explains the shortening of the C−N bonds (8.6 pm, see Table 1), but suggests a larger increase in the N−N bond length than

found at the CASSCF level (0.7 pm). In fact, according to the ELF picture, the N−N bond of the S_1 state should be close to a single bond, as the population of the V(N,N) basin is close to 2 e. The C−N bond should be strengthened upon excitation since the population of the V(C,N) basin increases from 2.08 to 2.55 e. Compared with the ground state, rotation in the S_1 state will thus be more facile around the N−N bond and more hindered around the C−N bond, which explains the stage-wise variation of the dihedral angles depicted in Figure 6. Qualitatively, both the MO and ELF pictures suggest a greater lengthening of the N−N bond upon excitation than actually found, but it is only the ELF analysis that accounts for the shortening of the C−N distance and the associated features in Figure 6.

We now address the role of in-phase and out-of phase rotation of the phenyl rings during the *trans*-to-*cis* photoreaction. When going from the MECI with a CNNC dihedral of ca. 90° to *c*AB with a CNNC dihedral of ca. 0°, there will be a steric clash of the phenyl rings if the orientation of these rings is kept fixed. This clash can be avoided by an in-phase rotation of the phenyl groups, which will thus favor the *c*AB pathway. Conversely, out-of phase rotation will tend to increase the steric hindrance and thus favor the *t*AB channel. To investigate this issue in more detail, we have estimated the angular rotation velocity of the phenyl rings at the hopping points by monitoring the change of the corresponding N−N−Ph dihedral. To remove the effects of ring deformations in the simulation, the phenyl rings were fitted to their least-squares plane. In the majority of trajectories (ca. 60%) the rings rotate out-of-phase at the hopping point. However, looking at the distinct photoproducts, we find that 76% (67%) of the *c*AB (*t*AB) trajectories arrive at the hopping point with an in-phase (out-of-phase) rotation of the phenyl rings (see Supporting Information), which is more than just accidental. A complete blocking of the out-of-phase ring motion may thus ideally lead to a substantial gain in *cis* photoproduction (34% vs 17%, see Table S2 in the Supporting Information).

These findings suggest that the phenyl ring rotation is a coordinate which, at least to some extent, will have an influence on the outcome of the photoreaction. For further analysis, we have performed computational experiments with special initial conditions. We have run dynamical simulations where this specific mode (v_{Phe}) was vibrationally excited, while all other modes were kept frozen (by neglecting their zero-point energy, ZPE). The computed frequency of v_{Phe} is very low (22 cm^{-1} in S_0), and we have therefore excited this mode into the ninth vibrational level to provide a reasonable amount of vibrational energy (around 200 cm^{-1}). Since the N_2 rotation is an important mode to reach the intersection seam (see above), we have also checked the effects of exciting this mode (v_{N_2}, 213 cm^{-1} in S_0) to the second vibrational level (with all other modes frozen). Finally, we have also run simulations with the v_{Phe} and v_{N_2} modes being excited (as above) and the remaining modes either frozen or in their vibrational ground state (i.e., including their ZPE). Table 2 gives a summary of the results.

The quantum yield for *c*AB is almost doubled (30%) when only the in-phase phenyl rotation is excited, with 85% of the trajectories maintaining their initial in-phase phenyl motion at the hop (see Supporting Information). The reaction is, however, significantly slower than in the standard simulation. The mean hopping time increases by almost 200 fs to 452 fs. Interestingly, the average time for the *trans*-to-*cis* reaction is

Table 2. Results for Different Sets of Vibrationally Excited Trajectories Compared with the Standard Simulation[a]

sample (see text)	$\langle E_k^0 \rangle$, kcal mol^{-1}	t, fs	t_{cis}, fs	t_{trans}, fs	% cis
standard	61 ± 12	258	312	247	17
all frozen but v_{Phe}	0.3 ± 0.2	452	385	443	30
all frozen but v_{Phe} and v_{N_2}	1.2 ± 0.7	353	348	356	38
all modes in the ground state, with v_{Phe} and v_{N_2} being excited	62 ± 12	200	251	188	20

[a]Given for each trajectory are the average initial kinetic energy ($\langle E_k^0 \rangle$), the average overall hopping time (t), the average hopping time for the trajectories yielding cAB (t_{cis}) and tAB (t_{trans}), and the percentage of cAB formed.

lower than that of the *trans*-to-*trans* process, i.e., there are less early tAB hops upon excitation of v_{Phe}. This further confirms the relation between phenyl ring in-phase rotation and photoproduct formation. Trajectories with only the v_{N_2} mode excited generally do not reach the crossing region within 800 fs and are not included in Table 2. Combined excitation of the v_{Phe} and v_{N2} modes increases the quantum yield to 38% and also speeds up the reaction compared to the simulation with excitation of only v_{Phe}. In this case, the mean hopping time increases by almost 100 fs compared to the standard sampling, and the fraction of trajectories which maintain their in-plane motion at the hop significantly drops to 56%. Finally, when the combined excitation of the v_{Phe} and v_{N_2} modes is investigated in the bath of the other modes (by including their ZPE), we note a significant speedup for both the *trans–cis* and *trans–trans* processes and a slight increase in the cAB yield compared with the standard simulation. The number of trajectories that maintain the in-plane phenyl torsion drops to 43%, indicating that the higher overall kinetic energy content works against the chosen initial in-phase phenyl rotation. In summary, these computational experiments provide evidence that the photoisomerization of azobenzene can be influenced by mode-specific initial excitations, both with regard to decay time and product distribution. These computational experiments are not exhaustive, of course, and it may well be that there are other modes relevant to this photoreaction.

CONCLUSIONS

The *trans*-to-*cis* photoisomerization of azobenzene has been studied by nonadiabatic surface hopping simulations at the OM2/MRCI level. Upon $n \rightarrow \pi^*$ photoexcitation, the molecule relaxes from the Franck–Condon region to the (S_1/S_0) seam along an essentially barrierless pathway (mainly involving the motion of the N–N fragment) and then hops to the ground state. Decay toward the *cis* photoproduct occurs from a narrow region of the seam (with CNNC dihedral angles between 80 and 120°), while the *trans* isomer can be generated all along the crossing region (also at larger CNNC dihedral angles that are reached earlier). Therefore, cAB is produced somewhat later than tAB (on average). As expected, there is no significant difference between the two possible chiral pathways when starting from planar tAB, contrary to the case of helically twisted cAB in the inverse *cis*-to-*trans* reaction.[43] Our simulations predict a quantum yield for cAB (17%) which agrees reasonably well with experimental estimates (20–25%), while the predicted average decay time (258 fs) underestimates the experimental value (340 fs).

We find oscillatory patterns in the population decay caused by periodic molecular motion. Such oscillations also appear in the *cis*-to-*trans* isomerization of azobenzene.[43] In both cases, the oscillatory pattern can be attributed to a single vibrational mode essentially consisting of N_2 rotation. This vibrational motion tends to pull in the phenyl rings and to bend the molecule toward the *cis* isomer, i.e., the photoisomerization proceeds by rotation of the N_2 moiety followed by phenyl rotation around the C–N bonds, rather than by exclusive rotation around the N=N bond. The *cis* isomer is produced most effectively when the phenyl rings rotate in phase. Simulations with specifically tailored initial conditions show that the cAB quantum yield can be enhanced by solely activating this motion. This effect is enhanced by also activating the N_2 rotation mode but is lost again when the ZPE of all other modes is included. These findings suggest mode-specific effects that may act in different stages of the reaction and require further exploration. Such effects have previously been identified in other photoisomerization processes, e.g., in the case of rhodopsin, which is guided through the intersection by hydrogen out-of-plane (HOOP) modes activated only very close to the crossing region.[79]

ASSOCIATED CONTENT

Ⓢ Supporting Information

Cartesian coordinates of stationary points, energy profiles, HOMO and LUMO plots, detailed ELF topology, and further analysis of trajectories. This material is available free of charge via the Internet at http://pubs.acs.org.

AUTHOR INFORMATION

Corresponding Author

*E-mail: thiel@kofo.mpg.de

Notes

The authors declare no competing financial interest.

ACKNOWLEDGMENTS

REFERENCES

(1) Natansohn, A.; Rolchon, P. *Chem. Rev.* **2002**, *102*, 4139–4176.
(2) Ichimura, K. *Chem. Rev.* **2000**, *100*, 1847–1874.
(3) Shibaev, V.; Bobrovsky, A.; Boko, N. *Prog. Polym. Sci.* **2003**, *28*, 729–836.
(4) Yu, Y.; Ikeda, T. *J. Photochem. Photobiol., C* **2004**, *5*, 247–265.
(5) Yu, Y.; Nakano, M.; Ikeda, T. *Nature* **2003**, *425*, 145–145.
(6) Holland, N. B.; Hugel, T.; Neuert, G.; Cattani-Scholz, A.; Renner, C.; Oesterhelt, D.; Moroder, L.; Seitz, M.; Gaub, H. E. *Macromolecules* **2003**, *36*, 2015–2023.
(7) Hugel, T.; Holland, N. B.; Cattani, A.; Moroder, L.; Seitz, M.; Gaub, H. E. *Science* **2002**, *296*, 1103–1106.
(8) Asakawa, M.; Ashton, P. R.; Balzani, V.; Brown, C. L.; Credi, A.; Matthews, O. A.; Newton, S. P.; Raymo, F. M.; Shipway, A. N.; Spencer, N.; Quick, A.; Stoddart, J. F.; White, A. J. P.; Williams, D. J. *Chem.–Eur. J.* **1999**, *5*, 860–875.
(9) Balzani, V.; Credi, A.; Marchioni, F.; Stoddart, J. F. *Chem. Commun.* **2001**, 1860–1861.
(10) Tamesue, S.; Takashima, Y.; Yamaguchi, H.; Shinkai, S.; Harada, A. *Angew. Chem., Int. Ed.* **2010**, *49*, 7461–7464.
(11) Yagai, S.; Nakajima, T.; Kishikawa, K.; Kohmoto, S.; Karatsu, T.; Kitamura, A. *J. Am. Chem. Soc.* **2005**, *127*, 11134–11139.

(12) Sakai, H.; Orihara, Y.; Kodashima, H.; Matsumura, A.; Ohkubo, T.; Tsuchiya, K.; Abe, M. *J. Am. Chem. Soc.* **2005**, *127*, 13454−13455.

(13) Kasha, M. *Discuss. Faraday Soc.* **1950**, *9*, 14−19.

(14) Zimmerman, G.; Chow, L.-Y.; Paik, U.-J. *J. Am. Chem. Soc.* **1958**, *80*, 3528−3531.

(15) Rau, H. *J. Photochem.* **1984**, *26*, 221−225.

(16) Bortolus, P.; Monti, S. *J. Phys. Chem.* **1979**, *83*, 648−652.

(17) Siampiringue, N.; Guyot, G.; Monti, S.; Bortolus, P. *J. Photochem.* **1987**, *37*, 185−188.

(18) Ronayette, J.; Arnaud, R.; Lebourgeois, P.; Lemaire, J. *Can. J. Chem.* **1974**, *52*, 1848−1857.

(19) Stegemeyer, H. *J. Phys. Chem.* **1962**, *66*, 2555−2560.

(20) Jaffe, H. H.; Orchin, M. *Theory and Application of Ultraviolet Spectroscopy*; Wiley: New York, 1962.

(21) Rau, H. *Angew. Chem. Int .Ed.* **1973**, *12*, 224−235.

(22) Bisle, H.; Römer, M.; Rau, H. *Ber. Bunsen. Physik. Chem.* **1976**, *80*, 301−305.

(23) Rau, H.; Lueddecke, E. *J. Am. Chem. Soc.* **1982**, *104*, 1616−1620.

(24) Fujino, T.; Arzhantsev, S. Y.; Tahara, T. *J. Phys. Chem. A* **2001**, *105*, 8123−8129.

(25) Cattaneo, P.; Persico, M. *Phys. Chem. Chem. Phys.* **1999**, *1*, 4739−4743.

(26) Monti, S.; Orlandi, G.; Palmieri, P. *Chem. Phys.* **1982**, *71*, 87−99.

(27) Biswas, N.; Umapathy, S. *Chem. Phys. Lett.* **1995**, *236*, 24−29.

(28) Granucci, G.; Persico, M. *Theor. Chem. Acc.* **2007**, *117*, 1131−1143.

(29) Ciminelli, C.; Granucci, G.; Persico, M. *Chem.—Eur. J.* **2004**, *10*, 2327−2341.

(30) Ishikawa, T.; Noro, T.; Shoda, T. *J. Chem. Phys.* **2001**, *115*, 7503−7512.

(31) Cembran, A.; Bernardi, F.; Garavelli, M.; Gagliardi, L.; Orlandi, G. *J. Am. Chem. Soc.* **2004**, *126*, 3234−3243.

(32) Wei-Guang Diau, E. *J. Phys. Chem. A* **2004**, *108*, 950−956.

(33) Tiago, M. L.; Ismail-Beigi, S.; Louie, S. G. *J. Chem. Phys.* **2005**, *122*, 094311.

(34) Conti, I.; Garavelli, M.; Orlandi, G. *J. Am. Chem. Soc.* **2008**, *130*, 5216−5230.

(35) Ciminelli, C.; Granucci, G.; Persico, M. *J. Chem. Phys.* **2005**, *123*, 174317.

(36) Toniolo, A.; Ciminelli, C.; Persico, M.; Martínez, T. J. *J. Chem. Phys.* **2005**, *123*, 234308.

(37) Pancur, T.; Renth, F.; Temps, F.; Harbaum, B.; Kruger, A.; Herges, R.; Nather, C. *Phys. Chem. Chem. Phys.* **2005**, *7*, 1985−1989.

(38) Ishii, K.; Takeuchi, S.; Tahara, T. *Chem. Phys. Lett.* **2004**, *398*, 400−406.

(39) Fuß, W.; Kosmidis, C.; Schmid, W. E.; Trushin, S. A. *Chem. Phys. Lett.* **2004**, *385*, 423−430.

(40) Böckmann, M.; Doltsinis, N. L.; Marx, D. *Phys. Rev. E* **2008**, *78*, 036101.

(41) Böckmann, M.; Doltsinis, N. L.; Marx, D. *J. Phys. Chem. A* **2009**, *114*, 745−754.

(42) Böckmann, M.; Marx, D.; Peter, C.; Site, L. D.; Kremer, K.; Doltsinis, N. L. *Phys. Chem. Chem. Phys.* **2011**, *13*, 7604−7621.

(43) Weingart, O.; Lan, Z.; Koslowski, A.; Thiel, W. *J. Phys. Chem. Lett.* **2011**, *2*, 1506−1509.

(44) Hoffmann, M.; Wanko, M.; Strodel, P.; König, P. H.; Frauenheim, T.; Schulten, K.; Thiel, W.; Tajkhorshid, E.; Elstner, M. *J. Am. Chem. Soc.* **2006**, *128*, 10808−10818.

(45) Lan, Z. G.; Fabiano, E.; Thiel, W. *ChemPhysChem* **2009**, *10*, 1225−1229.

(46) Kazaryan, A.; Lan, Z. G.; Schafer, L. V.; Thiel, W.; Filatov, M. *J. Chem. Theory Comput.* **2011**, *7*, 2189−2199.

(47) Lan, Z. G.; Lu, Y.; Fabiano, E.; Thiel, W. *ChemPhysChem* **2011**, *12*, 1989−1998.

(48) Welke, K.; Framcke, J. S.; Watanabe, H. C.; Hegemann, P.; Elstner, M. *J. Phys. Chem. B* **2011**, *115*, 15119−15128.

(49) Dewar, M. J. S.; Hashmall, J. A.; Venier, C. G. *J. Am. Chem. Soc.* **1968**, *90*, 1953−1957.

(50) Weber, W. Ph.D. Thesis, University of Zürich, 1996.

(51) Weber, W.; Thiel, W. *Theor. Chem. Acc.* **2000**, *103*, 495−506.

(52) Otte, N.; Scholten, M.; Thiel, W. *J. Phys. Chem. A* **2007**, *111*, 5751−5755.

(53) Thiel, W. *MNDO program:* version 6.1; Max-Planck-Institut für Kohlenforschung: Mülheim, Germany, 2007.

(54) Koslowski, A.; Beck, M. E.; Thiel, W. *J. Comput. Chem.* **2003**, *24*, 714−726.

(55) *Conical Intersections: Electronic Structure, Dynamics and Spectroscopy*; Domcke, W.; Yarkony, D. R.; Köppel, H., Eds.; World Scientific Publishing: Singapore, 2004.

(56) Keal, T.; Koslowski, A.; Thiel, W. *Theor. Chem. Acc.* **2007**, *118*, 837−844.

(57) Tully, J. C. *J. Chem. Phys.* **1990**, *93*, 1061−1071.

(58) Fabiano, E.; Keal, T. W.; Thiel, W. *Chem. Phys.* **2008**, *349*, 334−347.

(59) Granucci, G.; Persico, M. *J. Chem. Phys.* **2007**, *126*, 134114.

(60) Wigner, E. *Phys. Rev.* **1932**, *40*, 749−759.

(61) Verlet, L. *Phys. Rev.* **1967**, *159*, 98−103.

(62) Barbatti, M.; Granucci, G.; Persico, M.; Ruckenbauer, M.; Vazdar, M.; Eckert-Maksic, M.; Lischka, H. *J. Photochem. Photobiol., A* **2007**, *190*, 228−240.

(63) Silva-Junior, M. R.; Thiel, W. *J. Chem. Theory Comput.* **2010**, *6*, 1546−1564.

(64) Pierloot, K.; Dumez, B.; Widmark, P.-O.; Roos, B. O. *Theor. Chem. Acc.* **1995**, *90*, 87−114.

(65) Aquilante, F.; De Vico, L.; Ferré, N.; Ghigo, G.; Malmqvist, P.-Å.; Neogrády, P.; Pedersen, T. B.; Pitoňák, M.; Reiher, M.; Roos, B. O.; Serrano-Andrés, L.; Urban, M.; Veryazov, V.; Lindh, R. *J. Comput. Chem.* **2010**, *31*, 224−247.

(66) Becke, A. D.; Edgecombe, K. E. *J. Chem. Phys.* **1990**, *92*, 5397−5403.

(67) Silvi, B. *Phys. Chem. Chem. Phys.* **2004**, *6*, 256−260.

(68) Kohout, M. *DGrid*, version 4.6; Radebeul, Germany, 2011.

(69) Andersson, J.-Å.; Petterson, R.; Tegnér, L. *J. Photochem.* **1982**, *20*, 17−32.

(70) Lednev, I. K.; Ye, T. Q.; Matousek, P.; Towrie, M.; Foggi, P.; Neuwahl, F. V. R.; Umapathy, S.; Hester, R. E.; Moore, J. N. *Chem. Phys. Lett.* **1998**, *290*, 68−74.

(71) Tsuji, T.; Takashima, H.; Takeuchi, H.; Egawa, T.; Konaka, S. *J. Phys. Chem. A* **2001**, *105*, 9347−9353.

(72) Mostad, A.; Rømming, C. *Acta Chem. Scand.* **1971**, *25*, 3561−3568.

(73) Pederzoli, M.; Pittner, J.; Barbatti, M.; Lischka, H. *J. Phys. Chem. A* **2011**, *115*, 11136−11143.

(74) Kurita, N.; Tanaka, S.; Itoh, S. *J. Phys. Chem. A* **2000**, *104*, 8114−8120.

(75) Wachtveitl, J.; Nägele, T.; Puell, B.; Zinth, W.; Krüger, M.; Rudolph-Böhner, S.; Oesterhelt, D.; Moroder, L. *J. Photochem. Photobiol., A* **1997**, *105*, 283−288.

(76) Gagliardi, L.; Orlandi, G.; Bernardi, F.; Cembran, A.; Garavelli, M. *Theor. Chem. Acc.* **2004**, *111*, 363−372.

(77) *Stereochemistry of Organic Compounds*; Eliel, E. L., Wilen, S. H., Eds.; Wiley-Interscience: New York, 1994.

(78) Satzger, H.; Spörlein, S.; Root, C.; Wachtveitl, J.; Zinth, W.; Gilch, P. *Chem. Phys. Lett.* **2003**, *372*, 216−223.

(79) Weingart, O.; Altoè, P.; Stenta, M.; Bottoni, A.; Orlandi, G.; Garavelli, M. *Phys. Chem. Chem. Phys.* **2011**, *13*, 3645−3648.

G

dx.doi.org/10.1021/ct300303s | *J. Chem. Theory Comput.* XXXX, XXX, XXX−XXX